Electrochemical and Spectroelectrochemical Characterization of (5,10,15,20-Tetrakis(1-methyl-4-pyridyl)porphinato)manganese(III) Chloride, $[(TMpyP)Mn^{III}Cl]^{4+}(Cl^-)_4$, in *N,N*-Dimethylformamide

Eric Van Caemelbecke, Włodzimierz Kutner,† and Karl M. Kadish*

Department of Chemistry, University of Houston, Houston, Texas 77204-5641

Received September 10, 1992

The electrochemical and spectroelectrochemical properties of (5,10,15,20-tetrakis(1-methyl-4-pyridyl)porphinato)-manganese(III) chloride, $[(TMpyP)Mn^{III}Cl]^{4+}(Cl^-)_4$, were studied by conductometry, cyclic voltammetry (CV), rotating disk electrode voltammetry, coulometry, thin-layer UV–visible spectroelectrochemistry, and ESR spectroscopy in *N,N*-dimethylformamide (DMF). The electrochemical behavior of $[(TMpyP)Mn^{III}Cl]^{4+}(Cl^-)_4$ is largely dependent on the concentration of tetra-*n*-butylammonium perchlorate (TBAP) and/or lithium chloride in solution, the potential scan rate, and the temperature. From three to five electroreduction CV peaks are observed between +0.40 and −1.40 V vs SCE under different experimental conditions. In 0.1 M TBAP the first electroreduction occurs at $E_{1/2}$ = +0.11 V and involves a quasireversible metal-centered one-electron transfer. The second electroreduction occurs at $E_{1/2}$ = −0.69 V and involves two electrons which are transferred to the conjugated porphyrin macrocycle. Three subsequent two-electron electroreductions, centered at the 1-methyl-4-pyridyl groups of the macrocycle, are observed between −0.90 and −1.12 V. These electroreductions are accompanied by chloride dissociation equilibria which are discussed in terms of a "double-box" mechanism.

Introduction

Positively charged $[(TMpyP)M]^{n+}$ metalloporphyrins, where M is a central metal in oxidation state II or III and TMpyP represents 5,10,15,20-tetrakis(1-methyl-4-pyridyl)porphyrin, have been studied for several years.[1-23] These metal complexes have also attracted recent interest because of their biological importance. Infrared and Raman spectroscopies,[12] as well as electrochemistry,[10,13] reveal strong interactions of some of these metalloporphyrins with DNA, and the zinc, manganese, and nickel metalloporphyrins have been utilized to probe the binding sites of nucleosides, nucleotides and DNA.[14,15]

All positively charged "tetrakis(*N*-methylpyridyl)" metalloporphyrins are readily electroreducible and their electrochemistry has been reported in both water[7,16-18] and polar organic solvents.[19-21] The Cu(II), Zn(II), and VO(IV) metalloporphyrins are present as monomers in *N,N*-dimethylformamide (DMF). They are reversibly electroreduced by a total of six electrons in three reversible two-electron transfer steps.[19] The first electroreduction involves a transfer of two electrons to the conjugated porphyrin ring, while the two subsequent electroreductions occur at the four 1-methyl-4-pyridyl groups of the macrocycle. Monomeric $[(TMpyP)Co]^{4+}$ is also electroreduced by a total transfer of six electrons,[20] but the first two occur in separate one-electron transfer steps. Dimerization has been proposed for some $[(TMpyP)M]^{n+}$ complexes in aqueous solutions,[22] and this is also the case for $[(TMpyP)Ni^{II}]$ in DMF.[21]

The electrochemistry of $[(TMpyP)Mn^{III}]^{5+}$ has been studied in water, but very little else is known about the electrochemistry of this complex in nonaqueous solvents.[7] The Mn(III/II) electroreduction of $[(TMpyP)Mn^{III}ClO_4]^{4+}(ClO_4^-)_4$ in DMF was described in a brief report in which it was also suggested that the second electroreduction occurred at the porphyrin ring.[23] However, detailed electrochemical investigations were not reported and no spectroscopic data were provided to confirm this assignment.

The present work describes the extensive electrochemistry of $[(TMpyP)Mn^{III}Cl]^{4+}(Cl^-)_4$ in DMF and also provides the UV–visible and ESR characteristics of the first three electroreduction products. The second electroreduction of $[(TMpyP)Mn^{III}]^{5+}$ in water is accompanied by hydrogenation of the porphyrin macrocycle,[16] and this prevented the investigation of subsequent electrochemical processes of this metalloporphyrin. This side reaction does not occur in DMF, a weakly polar aprotic solvent, and the further electrode reactions as well as dissociation equilibria of both the chloride axial ligand and the chloride counteranions can then be easily investigated.

* Author for correspondence.
† On leave from the Institute of Physical Chemistry, Polish Academy of Sciences, Kasprzaka 44, 01-224 Warsaw, Poland.

(1) Pasternack, R. F.; Francesconi, L.; Raff, D.; Spiro, E. *Inorg. Chem.* **1973**, *12*, 2606.
(2) Forshey, P. A.; Kuwana, T. *Inorg. Chem.* **1981**, *20*, 693.
(3) Harriman, A.; Porter, G.; Richoux, M. C. *J. Chem. Soc., Faraday Trans. 2* **1981**, *77*, 1939.
(4) Neta, P. *J. Phys. Chem.* **1981**, *85*, 3678.
(5) Kalyanasundaram, K.; Neumann-Spallart, M. *J. Phys. Chem.* **1982**, *86*, 5163.
(6) Carnieri, N.; Harriman, A.; Porter, G. *J. Chem. Soc., Dalton. Trans.* **1982**, 931.
(7) Harriman, A. *J. Chem. Soc., Dalton. Trans.* **1984**, 141.
(8) Kalyanasundaram, K. *Inorg. Chem.* **1984**, *23*, 2453.
(9) Lin, C. Y.; Su, Y. O. *J. Electroanal. Chem. Interfacial Electrochem.* **1989**, *265*, 305.
(10) Rodriguez, M.; Bard, A. J. *Inorg. Chem.* **1992**, *31*, 1129.
(11) Kellar, K. E.; Foster, N. *Inorg. Chem.* **1992**, *31*, 1353.
(12) Nonaka, Y.; Lu, D. S.; Dwivedi, A.; Strommen, D. P.; Nakamoto, K. *Biopolymers* **1990**, *29*, 999.
(13) Rodriguez, M.; Kodadek, T.; Torres, M.; Bard, A. J. *Bioconjugate Chem.* **1990**, *2*, 123.
(14) Pasternack, R. F.; Gibbs, E. J.; Gaudemer, A.; Antebi, A.; Bassner, S.; De Poy, L.; Turner, D. H.; Williams, A.; Laplace, F.; Lansard, M. H.; Merienne, C.; Perree-Fauvet, M. *J. Am. Chem. Soc.* **1985**, *107*, 8179.
(15) Strickland, J. A.; Marzilli, L. G.; Wilson, W. D.; Zon, G. *Inorg. Chem.* **1989**, *28*, 4191.
(16) Morehouse, K. M.; Neta, P. *J. Phys. Chem.* **1984**, *88*, 1575.
(17) Hambright, P.; Neta, P.; Richoux, M. C.; Abou-Gamra, Z.; Harriman, A. *J. Photochem.* **1987**, *36*, 255.
(18) Baral, S.; Hambright, P.; Neta, P. *J. Phys. Chem.* **1984**, *88*, 1595.
(19) Kadish, K. M.; Araullo, C.; Maiya, G. B.; Sazou, D.; Barbe, J.-M.; Guilard, R. *Inorg. Chem.* **1989**, *28*, 2528.
(20) Araullo-McAdams, C.; Kadish, K. M. *Inorg. Chem.* **1990**, *29*, 2749.
(21) Kadish, K. M.; Sazou, D.; Liu, Y. M.; Saoibi, A.; Ferhat, M.; Guilard, R. *Inorg. Chem.* **1988**, *27*, 686.
(22) Neta, P.; Richoux, M. C.; Harriman, A.; Baral, S.; Hambright, P. *J. Phys. Chem.* **1986**, *90*, 2467.
(23) Hambright, P., Williams, R. F. X., Eds. *Porphyrin Chemistry Advances*, Ann Arbor Science: Ann Arbor, MI, 1979; pp 284–292.

0020-1669/93/1332-0438$04.00/0

Experimental Section

Chemicals. [(TMpyP)Mn^{III}Cl]$^{4+}$(Cl$^-$)$_4$ (Midcentury Chemical Co., Posen, IL) was used without further purification. Anhydrous, argon-packed *N,N*-dimethylformamide, DMF, (Aldrich Chemical Co., Milwaukee, WI) and methyl alcohol (Mallinckrodt, Paris, KY) were used as received. Tetra-*n*-butylammonium perchlorate, TBAP (Fluka Chemie AG, Buchs, Switzerland), was twice recrystallized from absolute ethanol and dried in vacuum at 40 °C prior to use.

Instrumentation. Conductivity measurements were performed with a Model 31 Conductivity Bridge (Yellow Springs Instrument Co., Inc., Yellow Springs, OH) equipped with a conductivity cell with a 0.1 cm^{-1} cell constant.

Cyclic voltammetry (CV), controlled potential coulometry, and rotating disk electrode (RDE) voltammetry were carried out in a conventional three-electrode cell with a Model 173 potentiostat/galvanostat equipped with a Model 173 digital coulometer (EG&G Princeton Applied Research Corp., Princeton, NJ) or a Model EC225 2A voltammetric analyzer (IBM Instruments, Danbury, CT). Platinum gauze was used as the working electrode for controlled-potential coulometry while either a 0.071 cm^2 area GC-30 glassy-carbon disk (Tokai Carbon, Inc., Japan) or a 0.008 cm^2 area platinum disk were used as the working electrodes for CV. A platinum wire served as the counter electrode. The reference electrode was a homemade saturated calomel electrode (SCE). It was separated from the bulk solution with a fritted glass bridge containing the solvent/supporting electrolyte mixture. RDE voltammetry was performed with a MSR Speed Control Unit (Pine Instrument Co., Grove City, PA). A 0.198 cm^2 area platinum RDE was purchased from Pine Instrument Co. All potentials are referenced to the SCE. A 0.2 M TBAP solution was used as the supporting electrolyte for bulk electrolyses and spectroelectrochemical measurements, while 0.1 M TBAP was used for voltammetric measurements.

UV–visible spectra of the initial metalloporphyrin complex were recorded with a Model 9430 UV–visible spectrophotometer (IBM Instruments Inc., Danbury, CT) at ±1-nm resolution while in situ thin-layer UV–visible spectra of both the initial metalloporphyrin and its electroreduced products were recorded with a Model TN-6500 rapid scan spectrophotometer/multichannel analyzer (Tracor Northern, Middleton, WI) at ±0.6-nm resolution. A large area platinum grid served as the working electrode in the utilized thin-layer spectroelectrochemical cell.[24]

ESR spectra were recorded with a Model ER 100E Spectrometer (Brüker, Billerica, MA). The *g* values were calculated with respect to diphenylpicrylhydrazide (DPPH), $g = 2.0037 \pm 0.0002$.[25] Low-temperature measurements were performed with a stream of nitrogen passing through a heat exchanger immersed in liquid nitrogen.

Results and Discussion

Characterization of Initial Metalloporphyrin, [(TMpyP)-Mn^{III}Cl]$^{4+}$(Cl$^-$)$_4$, in DMF. The structural formula of the initial metalloporphyrin with four dissociated equatorial chloride counteranions, [(TMpyP)Mn^{III}Cl]$^{4+}$, is presented in structure I.

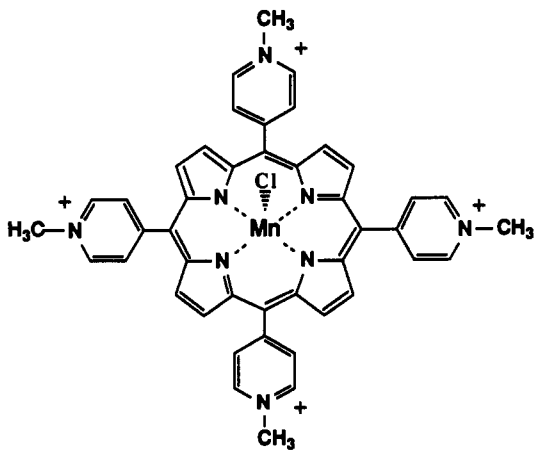

I

(24) Lin, X. Q.; Kadish, K. M. *Anal. Chem.* **1985**, *57*, 1498.
(25) Drago, R. S. *Physical Methods in Chemistry*; W. B. Saunders: Philadelphia, PA, 1977; p 324.

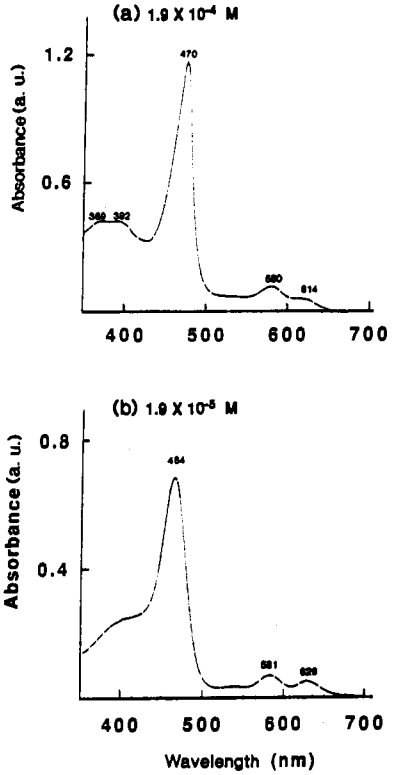

Figure 1. Electronic absorption spectra of DMF solutions containing (a) 1.9×10^{-4} M (0.1 cm cuvette) and (b) 1.9×10^{-5} M (0.5 cm cuvette) {[(TMpyP)Mn^{III}Cl]$^{4+}$(Cl$^-$)$_n$}$^{4-n}$.

Results of conductivity measurements in DMF (not shown) indicate that the metalloporphyrin is partially dissociated, but the number of chloride counteranions released could not be precisely determined due to difficulties with calibration of the system vs chlorides. Therefore, the initial metalloporphyrin species in solution is denoted as {[(TMpyP)Mn^{III}Cl]$^{4+}$(Cl$^-$)$_n$}$^{4-n}$, where $2 \le n \le 4$. Three chloride anions at most are dissociated upon electroreduction as discussed in later sections.

UV–visible spectra of the initial metalloporphyrin at two different concentrations in DMF are presented in Figure 1. The spectrum of the more concentrated, 1.9×10^{-4} M, solution displays a split Soret band composed of broad overlapping peaks at 369 and 392 nm, a charge-transfer band at 470 nm, and two visible bands located at 580 and 614 nm (Figure 1a). The spectrum of the more dilute, 1.9×10^{-5} M, solution is slightly different. Namely, the Soret band is broader and its two overlapping peaks are almost completely merged (Figure 1b). Also, the charge-transfer band is blue shifted to 464 nm and the second visible band is red shifted to 629 nm. Only the position of the band at 581 nm is virtually the same at the two concentrations.

The concentration-dependent changes in the visible spectrum of {[(TMpyP)Mn^{III}Cl]$^{4+}$(Cl$^-$)$_n$}$^{4-n}$ are further depicted in Figure 2 in which spectra are presented for three different metalloporphyrin concentrations such that the concentration times the optical path length was constant. As described above, the position and molar absorptivity of the band at 580–581 nm is concentration independent, but the molar absorptivity of the other visible band markedly increases with a decrease of the metalloporphyrin concentration. Beer's law is obeyed for the visible band at 580 nm, but not for the band at 614–630 nm. Straight log *A* vs log *C* lines are obtained for both bands (Figure 3). The slope of the line for the 580-nm band is equal to 1.07 and is close to the theoretical value of 1.0, while that for the 630-nm band is much lower and is equal to 0.75. This spectral analysis is indicative of some chemical transformation of {[(TMpyP)Mn^{III}Cl]$^{4+}$(Cl$^-$)$_n$}$^{4-n}$ over the investigated concentration range. Moreover, the spectrum of 2.0×10^{-4} M {[(TMpyP)Mn^{III}Cl]$^{4+}$(Cl$^-$)$_n$}$^{4-n}$ in DMF under argon is different than that in DMF which was exposed

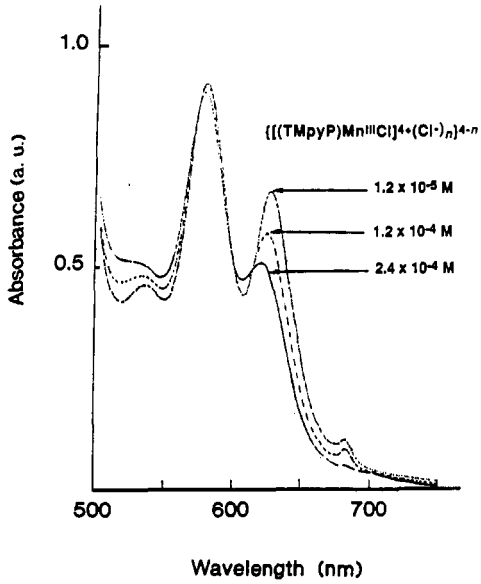

Figure 2. Electronic absorption spectra for different concentrations of {[(TMpyP)Mn^{III}Cl]$^{4+}$(Cl$^-$)$_n$}$^{4-n}$ in DMF. The concentration times the optical length was kept constant and equal to 1.2×10^{-4} M cm.

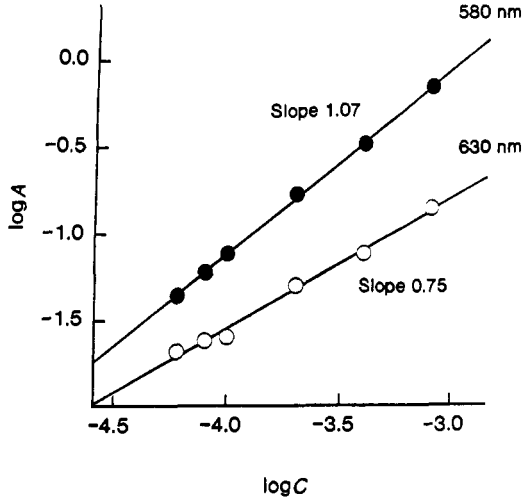

Figure 3. Logarithmic dependence of absorbance on concentration of {[(TMpyP)Mn^{III}Cl]$^{4+}$(Cl$^-$)$_n$}$^{4-n}$ in DMF at 580 (●) and 630 nm (○).

to air for a few days before the measurements. The spectrum obtained in DMF which had been in contact with air resembles the one observed at lower metalloporphyrin concentrations while the one in fresh, anhydrous, argon-packed DMF is similar to the spectrum obtained at the higher porphyrin concentrations. This may suggest that dimethylamine, which is produced in DMF when exposed to air,[26] binds to the manganese(III) center of the metalloporphyrin, causing the observed spectral changes. This hypothesis was confirmed by deliberate addition of diethylamine to fairly concentrated, 6×10^{-4} M, {[(TMpyP)Mn^{III}Cl]$^{4+}$(Cl$^-$)$_n$}$^{4-n}$ in fresh DMF. The addition of 240 equiv of diethylamine results in a spectrum which is similar to the one observed at the lowest metalloporphyrin concentration. It is well-known that ligands such as pyridines,[27] imidazoles,[28] and alcohols[29] axially bind to manganese(III) porphyrins, and it is therefore not surprising that the observed concentration-dependent changes would be due to formation of a dimethylamine-ligated manganese(III) porphyrin. Therefore, only fresh, anhydrous, argon-packed DMF was used

(26) (a) *Organic Solvents. Physical Properties and Methods of Purification*, 4th ed.; Riddick, J. A., Brunger, W. B., Sakano, T. K., Eds.; Wiley: New York, 1986; p 1085. (b) Mann, C. K. In *Electroanalytical Chemistry*; Bard, A. J., Ed.; Marcel Dekker: New York, 1969; p 57.
(27) Kadish, K. M.; Kelly, S. *Inorg. Chem.* **1979**, *18*, 2968.
(28) Kadish, K. M.; Kelly, S. L. *Inorg. Chem.* **1982**, *21*, 3631.
(29) Mu, X. H.; Schultz, F. A. *Inorg. Chem.* **1992**, *31*, 3351.

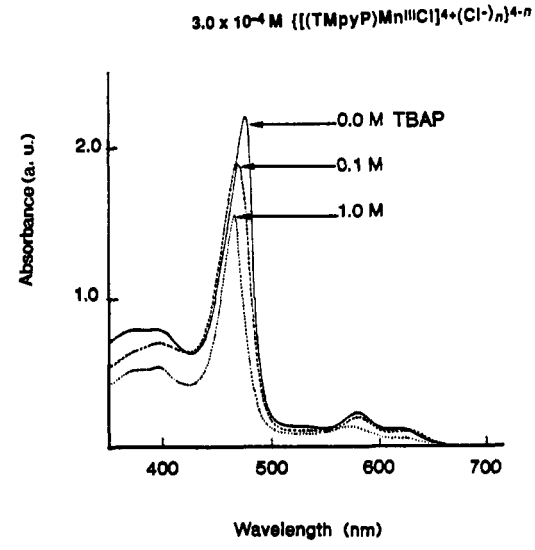

Figure 4. Electronic absorption spectra of 3.0×10^{-4} M {[(TMpyP)-Mn^{III}Cl]$^{4+}$(Cl$^-$)$_n$}$^{4-n}$ in DMF containing different concentrations of TBAP.

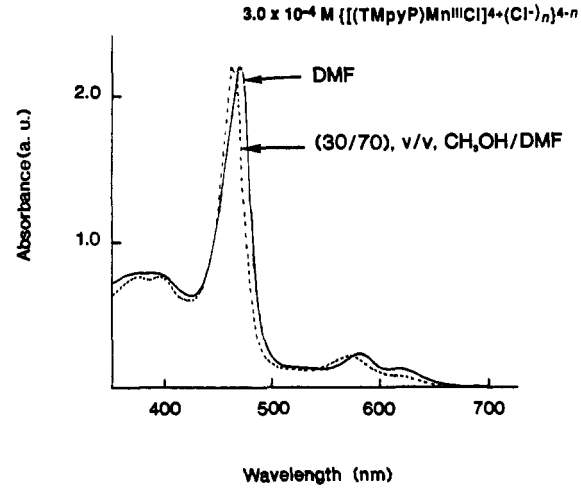

Figure 5. Electronic absorption spectra of 3.0×10^{-4} M {[(TMpyP)-Mn^{III}Cl]$^{4+}$(Cl$^-$)$_n$}$^{4-n}$ in DMF (—) and in CH_3OH/DMF, 30/70 (v/v) (- - -).

throughout all electrochemical and spectroelectrochemical studies. Also, the metalloporphyrin concentrations in electrochemical experiments were of the order of 1 mM, and this was sufficiently high to ensure that the fraction of metalloporphyrin ligated by the dimethylamine impurity was negligible.

The UV-visible spectral features of {[(TMpyP)-Mn^{III}Cl]$^{4+}$(Cl$^-$)$_n$}$^{4-n}$ also depend on the ionic strength of the solution. An increase of the TBAP concentration is accompanied by a decrease of all absorption bands and also by a blue shift of both the charge-transfer and visible bands (Figure 4). The spectrum of {[(TMpyP)Mn^{III}Cl]$^{4+}$(Cl$^-$)$_n$}$^{4-n}$ in DMF containing 1.0 M TBAP is similar to the spectrum of [(TMpyP)Mn^{III}]$^{5+}$ in water[30] where the counteranions of the metalloporphyrin are assumed to be completely dissociated.[7]

Figure 5 shows the spectrum of {[(TMpyP)Mn^{III}Cl]$^{4+}$(Cl$^-$)$_n$}$^{4-n}$ in DMF and also in a 30/70 (v/v), CH_3OH/DMF mixture. The addition of CH_3OH to a DMF solution of {[(TMpyP)-Mn^{III}Cl]$^{4+}$(Cl$^-$)$_n$}$^{4-n}$ results in a blue shift of both the charge-transfer and visible bands, as is the case for addition of CH_3OH to a 1,2-dichloroethane solution of (TPP)Mn^{III}Cl.[29] The spectrum in the CH_3OH/DMF mixture (Figure 5) resembles the one obtained in water[5,30] as well as the spectrum in DMF containing 1.0 M TBAP (Figure 4). This suggests that, under all three

(30) The UV-visible spectrum of {[(TMpyP)Mn^{III}Cl]$^{4+}$(Cl$^-$)$_n$}$^{4-n}$ in H_2O displays absorption bands at 377, 398, 462, and 559 nm.

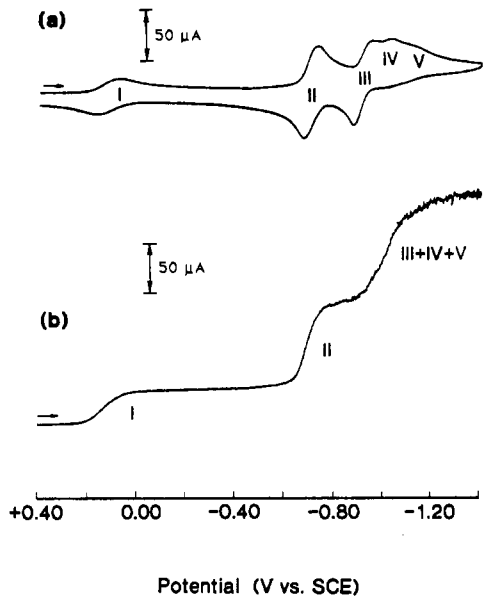

Figure 6. (a) Cyclic voltammogram (0.071 cm^2 glassy-carbon disk, scan rate 0.10 V s^{-1}) and (b) rotating disk electrode voltammogram (0.198 cm^2 area Pt disk, 1600 rpm) of 7.4 × 10^{-4} M {[(TMpyP)-Mn^{III}Cl]$^{4+}$(Cl$^-$)$_n$}$^{4-n}$ in DMF containing 0.1 M TBAP.

experimental conditions, the axial chloride ligand is dissociated from the metalloporphyrin.

Electrode Processes. The electroreduction of {[(TMpyP)-Mn^{III}Cl]$^{4+}$(Cl$^-$)$_n$}$^{4-n}$ was investigated by CV in the 0.05–0.50 V s^{-1} range of potential scan rate, v, and by RDE voltammetry at 1600 rpm. Thin-layer spectroelectrochemical and bulk coulometry measurements were also performed.

Five electroreductions are observed in the cyclic voltammogram of 0.74 mM {[(TMpyP)Mn^{III}Cl]$^{4+}$(Cl$^-$)$_n$}$^{4-n}$ in DMF containing 0.1 M TBAP (Figure 6a). They are labeled as processes I–V. The first two electroreductions are well-defined in the RDE voltammogram, but the last three (processes III–V) form an overlapped single step whose overall limiting current is slightly larger than that of process II (Figure 6b).

The separation between the anodic and cathodic peak potentials, $\Delta E_p = |E_{pa} - E_{pc}|$, for process I increases from 130 to 230 mV with increase of scan rate from 0.05 to 0.50 V s^{-1}. A plot of the cathodic peak current, i_{pc}, versus the square root of scan rate is linear, and its intercept is close to zero (not shown). Also a plot of log i_{pc} vs. log v is linear with a slope of 0.5 (not shown). Moreover, the ratio of the cathodic-to-anodic peak currents by CV is close to unity. All of these CV criteria are consistent with a quasireversible, diffusion-controlled electrode process. If one assumes that the diffusion coefficients of the reduced and oxidized forms of the metalloporphyrin are the same (values of D = (2.0 ± 0.3) × 10^{-6} cm^2 s^{-1} were calculated for the oxidized form) and that one electron is transferred (see below), then the standard rate constant of electron transfer is calculated as k_s = (1.3 ± 0.2) × 10^{-3} cm s^{-1} with the method of Nicholson.[31] This value agrees well with the one obtained in water.[7]

The cathodic peak current of process II also fulfills the CV criteria for a diffusion controlled process as described above, but the current is more than twice as high as that of process I. The ΔE_p separation for this process is scan rate independent and equal to 35 mV. Hence, process II is consistent with two closely-spaced diffusion-controlled reversible one-electron transfers.[32]

Because processes III–V are overlapped, the number of electrons transferred in each electroreduction could not be determined by either RDE voltammetry or by CV. Thin-layer and bulk controlled-potential coulometry measurements were therefore performed to determine the overall number of electrons transferred in all five processes.

The number of electrons transferred to {[(TMpyP)-Mn^{III}Cl]$^{4+}$(Cl$^-$)$_n$}$^{4-n}$ was determined upon exhaustive electroreduction at potentials more negative than processes I, II, and V. Both bulk controlled-potential and thin-layer coulometry result in the transfer of 0.8 ± 0.1 electron at –0.30 V (process I) while 3.0 ± 0.2 electrons are transferred at –0.80 V (processes I and II) by both coulometric techniques. Thin-layer coulometry at –1.40 V, a potential more negative than process V, resulted in an overall 5.0 ± 0.2 electrons transferred, while bulk controlled-potential coulometry, unexpectedly, resulted in only 4.1 ± 0.2 electrons. One may speculate that this rather low value is due to some chemical transformation in solution which manifests itself on a longer, bulk coulometry, time scale. However, it should be noted that the same number of electrons was recovered for each electroreduction upon electrooxidation at a potential more positive than the first electroreduction.

Electronic absorption spectra obtained during thin-layer controlled potential electroreduction of {[(TMpyP)-Mn^{III}Cl]$^{4+}$(Cl$^-$)$_n$}$^{4-n}$ at potentials more negative than processes I–III are shown in Figure 7. During the first electroreduction, the split Soret band disappears, the intensity of the charge-transfer band increases and the visible bands shift toward longer wavelengths (Figure 7a). The final spectrum is typical of a manganese(II) porphyrin.[33,34] There are no absorption bands between 650 and 750 nm in this spectrum, and this suggests that a metalloporphyrin π-anion radical is absent. Figure 8a presents the frozen solution ESR spectrum recorded at 136 K for the product of the first electroduction. There is a low-field six-line ^{55}Mn pattern (8-mT splitting) in this spectrum and the g values ($g_\perp$ = 5.914 and $g_\parallel$ = 1.981) are characteristic of a high spin (s = $^5/_2$) manganese(II) porphyrin.[35,36]

The UV–visible spectral changes observed during the second electroreduction, i.e, upon the potential step from –0.30 to –0.80 V (process II) are shown in Figure 7b. The charge-transfer band decreases substantially and shifts slightly from 463 to 468 nm. Also, an isosbestic point appears at 480 nm and there is a new broad band at 768 nm which resembles a band previously reported for the product of the two-electron electroreduction of [(TMpyP)M]$^{4+}$ (M = Zn, Cu, or VO)[19] at the porphyrin macrocycle. The ESR spectrum obtained at 136 K after bulk electrolysis of {[(TMpyP)Mn^{III}Cl]$^{4+}$(Cl$^-$)$_n$}$^{4-n}$ at –0.80 V is shown in Figure 8b. There are signals at $g_\parallel \approx 2$ and $g_\perp \approx 6$ but, in contrast to the spectrum in Figure 8a, twelve rather than six hyperfine lines can be distinguished at the higher g value. Similar spectra were reported previously for protein-bound manganese(II) protoporphyrins.[35] The change of the apoprotein from protoporphyrin IX to cytochrome c peroxidase resulted in an increase of the number of hyperfine lines from six to twelve for the signal at $g_\parallel \approx 6$. These hyperfine lines were attributed to a rhombic distortion of the axial ligand field around the manganese ion, induced by binding to the apoprotein. This distortion pushes the manganese(II) ion out of the plane of the porphyrin macrocycle. Similarly, the hyperfine structure of the spectrum shown in Figure 8b could also arise from such a rhombic distortion resulting from the charge increase on the conjugated porphyrin macrocycle. Thus, both the ESR and UV–visible spectroelectrochemical results point to a manganese(II) porphyrin which is reduced by two electrons at the conjugated porphyrin macrocycle.

A subsequent transfer of two electrons at –0.95 V (process III) gives rise to the UV–visible spectral changes shown in Figure 7c. During this electroreduction, the 468-nm band shifts to 424 nm, and there is a well-defined isosbestic point at 455 nm. The intensity of the band at 768 nm decreases, and the peak maximum

(31) Nicholson, R. S. *Anal. Chem.* **1965**, *37*, 1351.
(32) Polcyn, D. S.; Shain, I. *Anal. Chem.* **1966**, *38*, 370.
(33) Valentine, J. S.; Quinn, A. E. *Inorg. Chem.* **1976**, *15*, 1997.
(34) Perree-Fauvet, M.; Gaudemer, A.; Bonvoisin, J.; Girerd, J. J.; Boucly-Goester, C.; Boucly, P. *Inorg. Chem.* **1989**, *28*, 3533.
(35) Yonetani, T.; Drott, H. R.; Leigh, J. S.; Reed, G. H.; Waterman, M. R.; Asakura, T. *J. Biol. Chem.* **1970**, *245*, 2998.
(36) Hoffman, B. M.; Weschler, C. J.; Basolo, F. *J. Am. Chem. Soc.* **1976**, *98*, 5473.

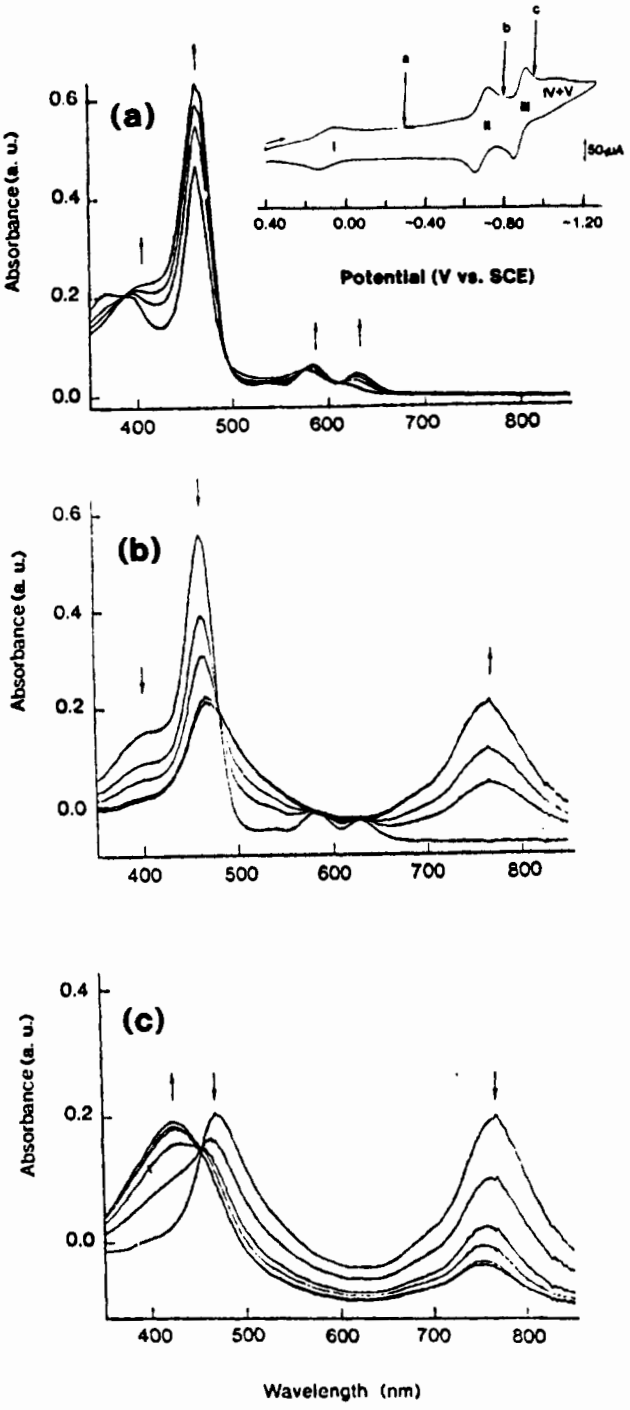

Figure 7. Time-resolved thin-layer electronic absorption spectra of 2.4 × 10^{-4} M $\{[(TMpyP)Mn^{III}Cl]^{4+}(Cl^-)_n\}^{4-n}$ in DMF containing 0.2 M TBAP upon a potential step from (a) +0.40 to −0.30 V, (b) −0.30 to −0.80 V, and (c) −0.80 to −0.95 V. The three steps are indicated by arrows in the inset voltammogram (platinum grid electrode, scan rate 0.020 V s^{-1}).

eventually shifts to 754 nm. The final spectrum is similar to the spectrum reported for the product of the third electroreduction of $[(TMpyP)Co^{II}]^{4+}$ in DMF.[20] The latter reduction is centered at the 1-methyl-4-pyridyl groups of the porphyrin and leads to $[(TMpyP)Co^{II}]^0$. By analogy, we conclude that the process III of the studied compound also involves an electroreduction of these groups.

The spectral changes recorded upon a potential step from −0.80 V to values more negative than process IV or V are the same as these presented in Figure 7c. We therefore conclude that processes III–V all involve electroreductions of the 1-methyl-4-pyridyl groups. Moreover, the fact that only two electrons are transferred in three discrete electrode processes between −0.80 and −1.40 V implies that there are three different forms of the triply-reduced metalloporphyrin in solution and that they are involved in

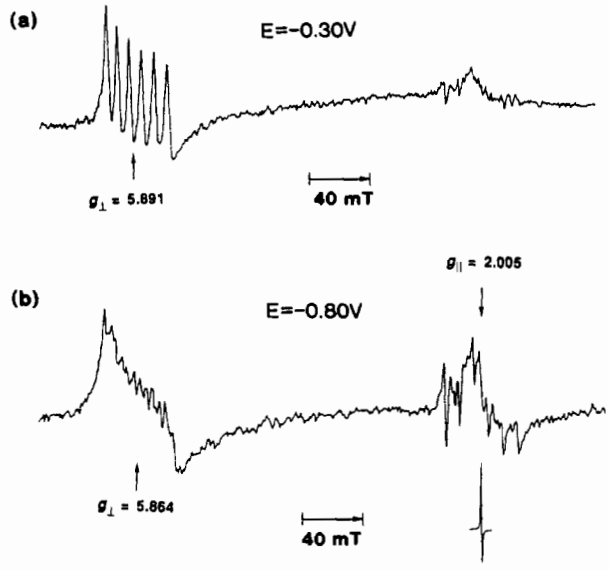

Figure 8. ESR spectra at 136 K of the product of exhaustive electroreduction of $\{[(TMpyP)Mn^{III}Cl]^{4+}(Cl^-)_n\}^{4-n}$ at (a) −0.30 V (process I) and (b) −0.80 V (process II).

electrochemical equilibria. These three different forms of the metalloporphyrin are electroreduced via processes III–V as discussed in the following section.

Chloride–Metalloporphyrin Electrochemical Equilibria. CV curves of 8 × 10^{-4} M $\{[(TMpyP)Mn^{III}Cl]^{4+}(Cl^-)_n\}^{4-n}$ in DMF containing 0.1 M TBAP at different scan rates and temperatures are presented in Figure 9. The relative heights and positions of the electroreduction peaks of processes I, II, and V are essentially independent of temperature (from −30 to +23 °C) and scan rate (from 0.05 to 0.50 V s^{-1}), but this is not the case for processes III and IV. The relative peak currents of process III decrease with either an increase of scan rate or a decrease of temperature, and this contrasts with the relative peak currents for process IV, which increase with increase of scan rate or decrease of temperature. Such behavior is typical of chemical equilibria accompanying the electrode processes. One such equilibrium might involve an exchange of the ClO_4^-/Cl^- counteranions on the 1-methyl-4-pyridyl groups of TMpyP. This postulate was verified by CV in solutions containing either different concentrations of TBAP or different TBAP/LiCl ratios at a constant ionic strength.

A series of CV experiments were performed with a DMF solution of 1.30 × 10^{-3} M $\{[(TMpyP)Mn^{III}Cl]^{4+}(Cl^-)_n\}^{4-n}$ containing concentrations of TBAP between 0.02 and 1.0 M. Cyclic voltammograms at three different concentrations of TBAP are shown in Figure 10a. As the concentration of TBAP increases, the relative electroreduction peak currents of process III increase, those of processes IV and V decrease and those of process II remain unchanged.

The electroreduction peak currents of processes I, III, IV, and V also depend on the LiCl concentration. An increase of the LiCl concentration at a constant ionic strength equal to 0.20 M (TBAP) results in a cathodic shift of the half-wave potential of process I (Figure 10b). A plot of $E_{1/2}$ vs log[Cl^-] for this process (not shown) is linear and its slope is −52 mV. This value may be compared to a theoretical slope of −59 mV if one chloride anion of the initial complex is released in process I. We believe that the dissociating chloride anion is the one bound to the central manganese(III) cation and that the proposed electroreduction product of process I is $\{[(TMpyP)Mn^{II}]^{4+}(Cl^-)_n\}^{4-n}$ as shown in eq 1. Obviously, the chloride dissociation which accompanies

$$\{[(TMpyP)Mn^{III}Cl]^{4+}(Cl^-)_n\}^{4-n} \overset{1e^-}{\rightleftarrows} \{[(TMpyP)Mn^{II}]^{4+}(Cl^-)_n\}^{4-n} + Cl^- \quad (1)$$

electron transfer in eq 1 is detected only in the presence of excess

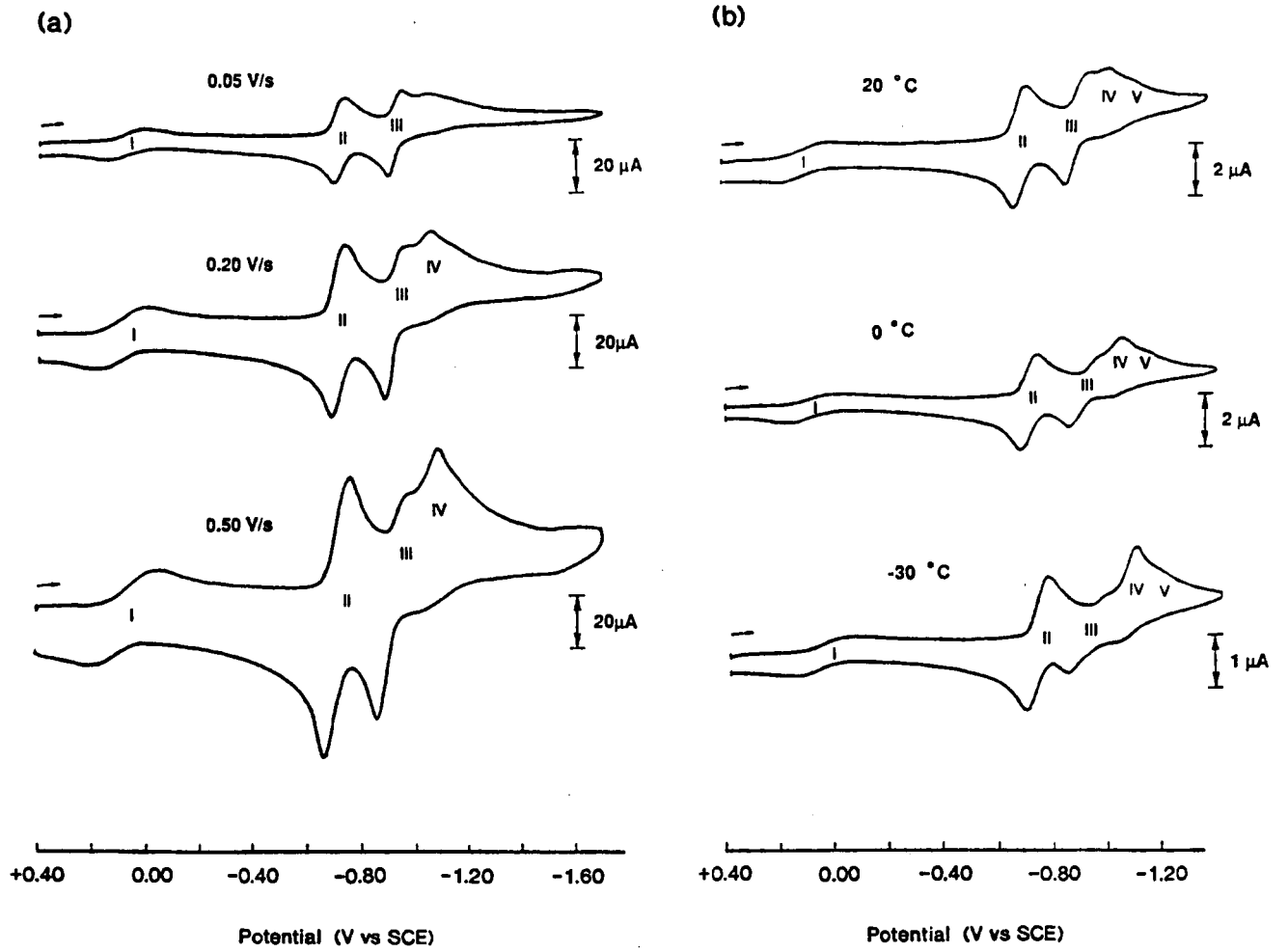

Figure 9. Cyclic voltammograms of 8.0×10^{-4} M $\{[(TMpyP)Mn^{III}Cl]^{4+}(Cl^-)_n\}^{4-n}$ in DMF, 0.1 M TBAP at (a) room temperature for scan rates of 0.05, 0.20, and 0.50 V s^{-1} and (b) a scan rate of 0.10 V s^{-1} and temperatures of +20, 0, and −30 °C.

Scheme I

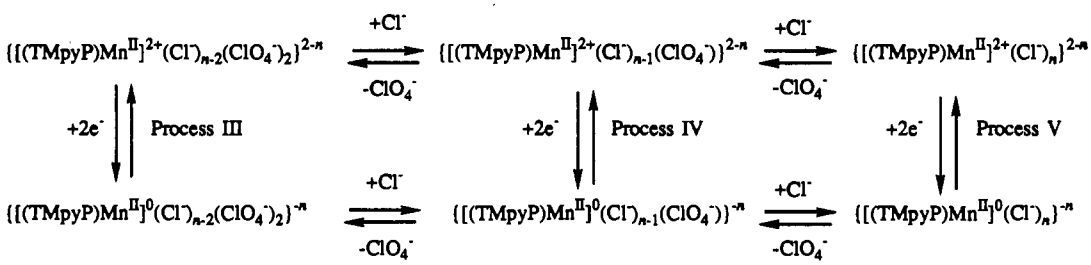

chloride in solution. If no Cl$^-$ is added to the solution, the dissociation equilibrium of the initial metalloporphyrin most likely is largely shifted toward $\{[(TMpyP)Mn^{III}]^{5+}(Cl^-)_n\}^{5-n}$. No $E_{1/2}$ dependence on Cl$^-$ concentration is observed for the second reduction, and this process is proposed to occur as shown in eq 2.

$$\{[(TMpyP)Mn^{II}]^{4+}(Cl^-)_n\}^{4-n} \overset{2e^-}{\rightleftharpoons} \{[(TMpyP)Mn^{II}]^{2+}(Cl^-)_n\}^{2-n} \quad (2)$$

Changes of the Cl$^-$/ClO$_4^-$ ratio do not affect the electroreduction peak currents of process II, but those of process III decrease with increase of the ratio such that the peak is totally gone in DMF containing 0.20 M LiCl (Figure 10b). At lower LiCl concentrations, the electroreduction peak currents of process III become scan rate independent (kinetic controlled) for $v \geq 0.10$ V s^{-1} and, at these scan rates, the log i_{pc} versus log [Cl$^-$] plot (not shown) is linear and its slope is equal to -1.1 ± 0.1. This indicates that a dissociation of one chloride ion precedes the electron transfer. The electroreduction peak current of process IV initially increases and then decreases with increase of the chloride concentration in solution while the currents of process V increase monotonically. Hence, it is plausible that a dissociation of one chloride counteranion precedes the electroreduction of process IV and that the product of process III is the electroactive species of process V. However, a detailed kinetic analysis could not be performed for the last two processes because of the proximity of these peaks to each other.

The CV results for $\{[(TMpyP)Mn^{III}Cl]^{4+}(Cl^-)_n\}^{4-n}$ in DMF containing different concentrations of TBAP or different Cl$^-$/ClO$_4^-$ ratios are consistent with the results obtained in DMF containing 0.1 M TBAP as well as those at different scan rates and different temperatures. They suggest that process II leads to three forms of the metalloporphyrin which are in equilibrium. Therefore, it is proposed that a different number of chloride counteranions are associated with each form of the metalloporphyrin and that processes III–V correspond to the electroreduction of each of them. Spectroelectrochemical data further confirm that the last three electroreduction processes involve the 1-methyl-4-pyridyl

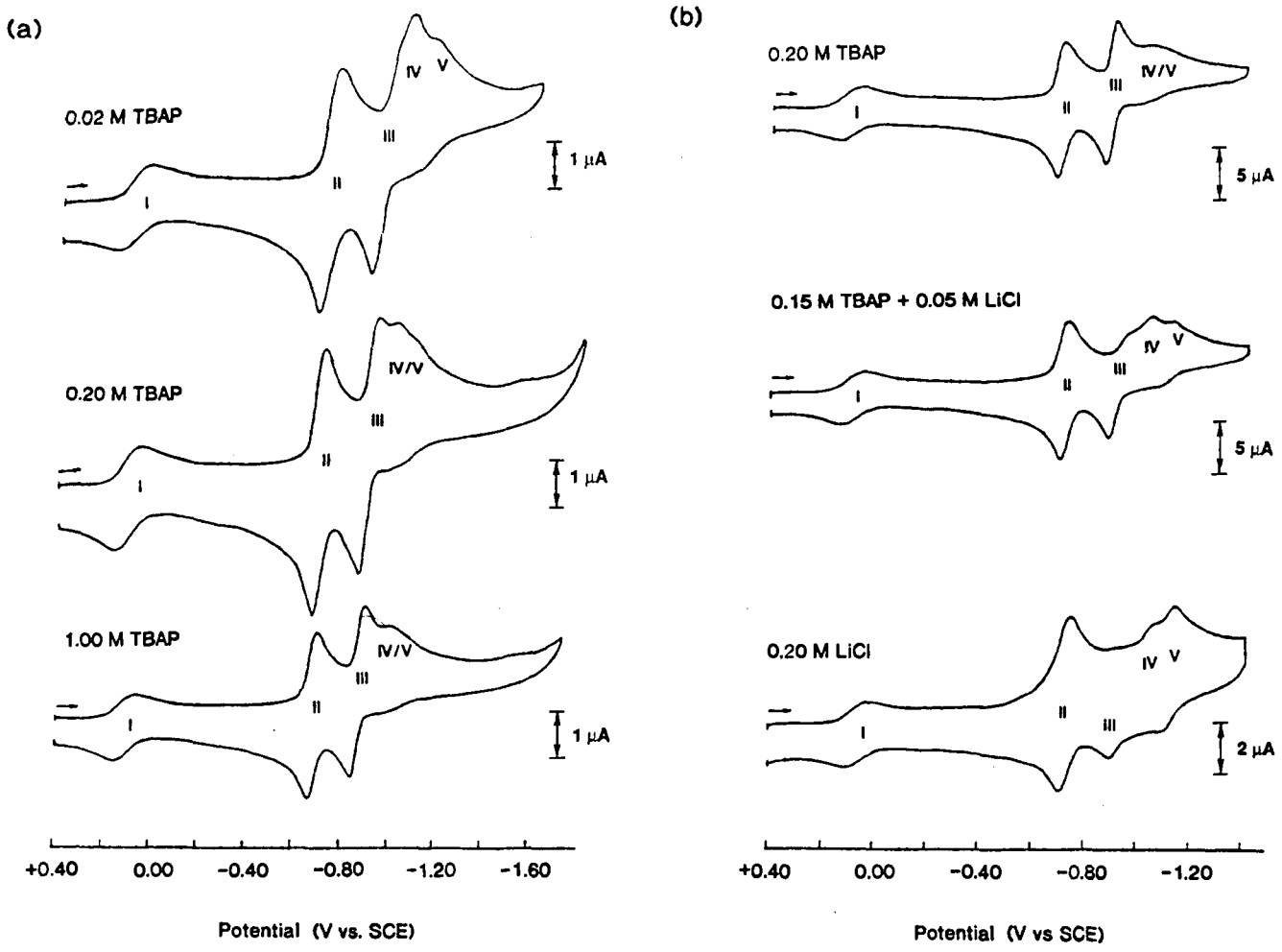

Figure 10. Cyclic voltammograms of (a) 1.3×10^{-3} M $\{[(TMpyP)Mn^{III}Cl]^{4+}(Cl^-)_n\}^{4-n}$ in DMF containing 0.02, 0.20, and 1.00 M TBAP and (b) 3.0×10^{-4} M $\{[(TMpyP)Mn^{III}Cl]^{4+}(Cl^-)_n\}^{4-n}$ in DMF containing different concentrations of LiCl at a constant ionic strength of 0.20 M (TBAP).

groups. Hence, the ligand dissociation equilibria most likely involve counteranions of these groups.

A proposed overall "double-box" mechanism of the electrochemical equilibria involving the last three processes is given in Scheme I. The equilibria in Scheme I are shifted to the right at higher chloride concentrations; i.e., processes IV and V are favored over process III while an opposite effect prevails at higher ClO_4^- concentrations (Figure 10). The most favorable conditions for process III are as follows: low scan rate, high temperature, high TBAP, and/or low chloride concentrations (Figures 9 and 10). Such a behavior is in accord with what is generally expected for a reversible electrochemical reduction of complex compounds in equilibrium; i.e., the electroreduction of $\{[(TMpyP)Mn^{II}]^{2+}(Cl^-)_{n-2}(ClO_4^-)_2\}^{2-n}$ should be easier (proceed at more positive potentials) than the electroreduction of $\{[(TMpyP)Mn^{II}]^{2+}(Cl^-)_n\}^{2-n}$, the metalloporphyrin with the larger number of chloride counteranions.

The high scan rate or low-temperature cyclic voltammograms (Figure 9) as well as the voltammograms obtained in DMF at low TBAP or high chloride concentrations (Figure 10) all indicate that $\{[(TMpyP)Mn^{II}]^{2+}(Cl^-)_{n-2}(ClO_4^-)_2\}^{2-n}$ is not the product formed after the total three-electron transfer to the initial metalloporphyrin in processes I and II. Under these conditions the equilibria are shifted toward the complex which is more rich in chlorides so that the electroreduction peak of process III is gone while that of process IV is enhanced. This suggests that $\{[(TMpyP)Mn^{II}]^{2+}(Cl^-)_{n-1}(ClO_4^-)\}^{2-n}$ is the predominant product of the three-electron transfer under our extreme experimental conditions, i.e., either at room temperature for a scan rate of 0.5 V s^{-1}, at −30 °C for a scan rate of 0.1 V s^{-1}, or at room temperature for solutions containing 0.20 M LiCl. Notably, a chloride–metalloporphyrin equilibria might also be present in solutions of the initial metalloporphyrin. Unfortunately, neither process I nor process II is sensitive to such equilibria and only processes III–V, which involve the 1-methyl-4-pyridyl substituents, provide evidence for these equilibria. Therefore, it is impossible to determine with the techniques utilized whether the loss of Cl^- occurs before or after the electron transfer in processes III–V.

Summary

Three sequential electroreduction processes of $\{[(TMpyP)Mn^{II}]^{4+}(Cl^-)_n\}^{4-n}$ are observed in DMF. They involve a total transfer of five electrons. Electrochemical, spectroelectrochemical, and ESR results indicate that the first process is a metal-centered one-electron transfer. Two electrons are transferred to the conjugated porphyrin ring in the second process. The third process involves chemical equilibria between three different chloride complexes of the manganese(II) porphyrin, all of which have been electroreduced by two electrons at the 1-methyl-4-pyridyl substituents of the TMpyP macrocycle. Finally, to our knowledge, the ESR spectrum of the electroreduction product of process II is the first reported of a manganese(II) porphyrin which has been reduced by two electrons at the conjugated porphyrin macrocycle.

Acknowledgment. The support of the National Science Foundation (Grant No. CHE-8822881), the National Institutes of Health (Grant No. GM-25172), and the Robert A. Welch Foundation (Grant E-680) is gratefully acknowledged.